Polymer 158 (2018) 381–390

Contents lists available at ScienceDirect

Polymer

journal homepage: www.elsevier.com/locate/polymer

Thermoplastic polyurethane-carbon black nanocomposite coating: Fabrication and solid particle erosion resistance

Mengyao Dong[a,b], Qiang Li[a], Hu Liu[a,*], Chuntai Liu[a,**], Evan K. Wujcik[c], Qian Shao[d], Tao Ding[e,***], Xianmin Mai[f,****], Changyu Shen[a], Zhanhu Guo[b,*****]

[a] School of Materials Science and Engineering, Key Laboratory of Materials Processing and Mold (Zhengzhou University), Ministry of Education, National Engineering Research Center for Advanced Polymer Processing Technology, Zhengzhou University, Zhengzhou, 450002, Henan, China
[b] Integrated Composites Laboratory (ICL), Department of Chemical & Biomolecular Engineering, University of Tennessee, Knoxville, TN, 37996, USA
[c] Materials Engineering and Nanosensors [MEAN] Laboratory, Department of Chemical and Biological Engineering, The University of Alabama, Tuscaloosa, AL, 35487, USA
[d] College of Materials Science and Engineering, Shandong University of Science and Technology, Qingdao, 266590, China
[e] College of Chemistry and Chemical Engineering, Henan University, Kaifeng, 475004, China
[f] School of Urban Planning and Architecture, Southwest Minzu University, Chengdu, 610041, China

HIGHLIGHTS

- Thermoplastic polyurethane nanocomposites were fabricated using co-coagulation plus compression molding technique.
- Uniform dispersion of CB nanoparticles effectively enhanced the tensile strength of the nanocomposites.
- The solid particle erosion behavior was characterized by different impact angles, velocities and time.
- The erosion rate showed an opposite trend to the tensile strength.

ARTICLE INFO

Keywords:
Carbon black
Thermoplastic polyurethane
Solid particle erosion

ABSTRACT

Carbon black (CB)/thermoplastic polyurethane (TPU) nanocomposites with a range of nanoparticle loadings were prepared successfully by using a joint co-coagulation technique and hot pressing. The presence of hydrogen bonding interactions between the CB particles and TPU chains was identified from the results of Fourier transform infrared (FT-IR) spectroscopy and differential scanning calorimetry (DSC). Uniform dispersion of CB particles throughout the TPU matrix improved the overall mechanical properties of the TPU nanocomposites, as compared with the neat TPU. The thermal conductivity and thermal stability of the CB/TPU nanocomposites were also found to be enhanced with increasing the CB loading. All samples exhibited a rapid increase of erosion rate with the impact velocity between 20 and 30 m/s. The largest and smallest erosion rates (ER) were observed at 30° and 90° impact angle, respectively, for all CB/TPU nanocomposites. This shows a typical ductile erosion behavior in this material. In addition, the ER (TPU-2CB > TPU-12CB > TPU > TPU-6CB) under all test conditions showed an opposite trend to the tensile strength. These results indicate that the CB/TPU nanocomposites are suitable for protective coatings.

1. Introduction

Wear usually causes serious damage to solid surfaces—due to the loss of material— arising from the relative movement of two interacting surfaces [1]. It has caused vast economic losses and many issues to the industrial sector. Statistically, solid particle erosion is one of the most

* Corresponding author.
** Corresponding author.
*** Corresponding author.
**** Corresponding author.
***** Corresponding author.
E-mail addresses: liuhu@zzu.edu.cn (H. Liu), ctliu@zzu.edu.cn (C. Liu), dingtao@henu.edu.cn (T. Ding), maixianmin@foxmail.com (X. Mai), zguo10@utk.edu (Z. Guo).

https://doi.org/10.1016/j.polymer.2018.11.003
Received 3 October 2018; Received in revised form 28 October 2018; Accepted 3 November 2018
Available online 04 November 2018
0032-3861/

common wear patterns, making up about more than 8% of all wear failures [2–4]. Since the first research paper about solid particle erosion was published in 1873 [5,6], numerous studies have been conducted to investigate the influencing factors of solid particle erosion, including impingement angle [7,8], impact velocity [9,10], particle flux rate [11,12], temperature [13], characteristics of eroded object, erodent properties such as shape, size, hardness, among others [14–17]. All these reveal the complexity of solid particle erosion phenomena. Although solid particle erosion has been widely studied, there are still a number of problems needed to be solved, including the fabrication of new materials to reduce wear and the study on an overall wear resistance mechanism.

Previous studies suggest that high hardness materials, such as metal and ceramic based materials, can provide excellent erosion resistance. However, they tend to be brittle, and the corrosion-resistant performances are still lacking [18]. Flexible polymer-based materials with high deformability and high resilience properties are able to absorb the impact energy and then release the energy again effectively when the deformation is restored. Therefore, the erosion of polymer based materials can be effectively reduced, showing better erosion resistance performance than that of metal and ceramic based materials [19]. Hence, the conventional metal and ceramic based anti-wear composites and coatings are gradually being replaced by polymer-based materials for their good processability, low cost, excellent wear resistance, and high impact absorbing ability [20–23]. Recently, typical anti-erosion polymer-based composites are now widely used for the fabrication of wind turbine blades, pipelines, automobile chassis, etc. [24–26].

Solid particle erosion of various thermoset and thermoplastic polymer-based composites has been investigated [27,28]. Among them, thermoplastic polyurethane (TPU), a segmented copolymer characterized by a sequence of hard and soft blocks, has attracted significant attention [29]. TPU has the mechanical properties of rubber and can be processed as a plastic [30]. Meanwhile, TPU exhibits high impact absorbing ability, a sufficiently high modulus, and excellent abrasion resistance. All these properties make TPU a suitable option for anti-erosion coatings or protective films. The properties of the TPU hinder the erosion processes dramatically, in an instance where high speed particles may hit the substrate surfaces [31–33].

Generally, the addition of suitable fillers into polymers could effectively enhance the mechanical and wear properties or even introduce other unique properties such as electrical conductivity, heat conductivity, magnetic properties and others [34–41]. For example, carbon-based fillers have been frequently used to enhance the mechanical properties as well as the wear resistance of the polymer matrix due to their excellent mechanical, self-lubricating effects, and wear-reducing effects [42,43]. Carbon black (CB) has exhibited enhanced effects on the wear resistance of polymer-based composites [44]. Compared with pure rubber, the wear resistance of EPDM/CB composites reduced by 30%–50% [45,46]. Meanwhile, the mechanical and wear resistance of composites was also observed to be increased dramatically with the addition of 10–30% volume percent of CF [47,48]. With the addition of CNTs, a significant improvement in the elastic modulus, failure strength, and fracture toughness of the polymer matrix can be observed. This is due to the excellent mechanical and thermal properties of CNTs, as well as the erosion rate of CF/epoxy composites, which could be reduced by 50% with the addition of the CNTs [49]. Graphite reinforced polymer composites showed obvious anti-erosion and self-lubricating effects in comparison with neat polymer under solid particle erosion test conditions [50]. The polyamide-6/graphite (15 wt %) exhibited 10 times more resistance, as compared with pure polyamide [42]. Graphene, an emerging ideal multifunctional nanofiller for polymer composites, also has received considerable interest for the fabrication of protecting films for various substances due to its excellent self-lubricating effects and wear-reducing effect in polymer composites [51]. Although a variety of carbon-based fillers can enhance the wear resistance of the polymer matrix, CB has the advantages of low cost and easy processing, and is often used as a reinforcing agent for polymer materials. Previously, a study on solid particle erosion behavior of TPU has been conducted [29], but the erosion behavior of CB/TPU nanocomposites has not been reported yet.

One of the important features that determines the improvement in the performance of the nanocomposites is the quality of the nanoparticle dispersion in the polymer matrix. Generally, matrix-filler compatibility, surface energy of the particles, and processing techniques are the key factors influencing the dispersion of fillers. Coagulation technique is an approach to precipitate the polymer from its solution by adding poor solvent of polymer (sometimes solvent extraction is used). In this work, CB/TPU mixture was added into the poor solvent methanol, TPU and CB/TPU nanocomposites precipitated together, keeping the uniform dispersion of CB in TPU matrix. Thus, “co-coagulation” was used to describe this process. Some recent papers use co-coagulation technique to fabrication polymer nanocomposites [31,52–56]. In the current study, CB/TPU nanocomposites with different CB loadings were prepared by a combination of co-coagulation technique and hot pressing. The interactions between the CB particles and molecular chain of the TPU were investigated by Fourier transform infrared (FT-IR) spectroscopy and differential scanning calorimetry (DSC). Thermogravimetric analysis (TGA) and thermal conductivity studies were conducted for the investigation of thermal stability and conductivity. The wear resistance of the CB/TPU nanocomposites was also investigated by testing the erosion rate (ER). The effects of CB content on the wear resistance and mechanical properties of nanocomposites were also systematically studied. This research will be critical in creating a database regarding the solid particle erosion behavior of CB/TPU nanocomposites, hence making the nanocomposites pertinent in fields where excellent wear resistance is required.

2. Experimental

2.1. Materials and chemicals

The materials used in this research include CB, TPU, dimethylformamide (DMF) and methanol. The CB (VXC-72) is a product of Cabot Co., Ltd. with a size about 30 nm. TPU (Elastollan 1185A) was obtained from BASF Co., Ltd. DMF and methanol were purchased from Zhiyuan Reagent Co., Ltd, Tianjin, China and used as received. CB and TPU were dried at 80 °C for 24 h under vacuum before usage and the others were used as received.

2.2. Preparation of CB/TPU nanocomposites

CB/TPU nanocomposites with different CB loadings were prepared using the co-coagulation technique and hot pressing (Fig. 1). First, 3.0 g of TPU was dissolved in 50 mL of DMF and stirred for 30 min at 40 °C. To disperse the CB particles homogenously, the CB particles were then mixed with 15 mL DMF and ultrasonicated for 30 min. These two solutions were mixed and ultrasonicated for another 30 min, and the flocculation of CB/TPU was obtained after adding the mixed solutions to 300 mL of methanol. Then, the filtered flocculate was dried for 24 h at 80 °C under vacuum, and pressed into a 0.4 mm film at 200 °C. The neat TPU film was also prepared in similar fashion, for comparison. Here, the CB/TPU nanocomposites were labeled as TPU-*x*CB, where *x* is the content (in wt%) of CB.

2.3. Characterization

All FT-IR spectra were obtained in the range from 500 to 4000 cm^{-1} and conducted in attenuated total reflection (ATR) mode on a Nicolet Nexus 870 instrument, the samples with dimensions of 20 mm × 4 mm × 0.4 mm were cut off from the CB/TPU nanocomposites films.

The DSC analysis tests were performed under N_2 at a flow rate of

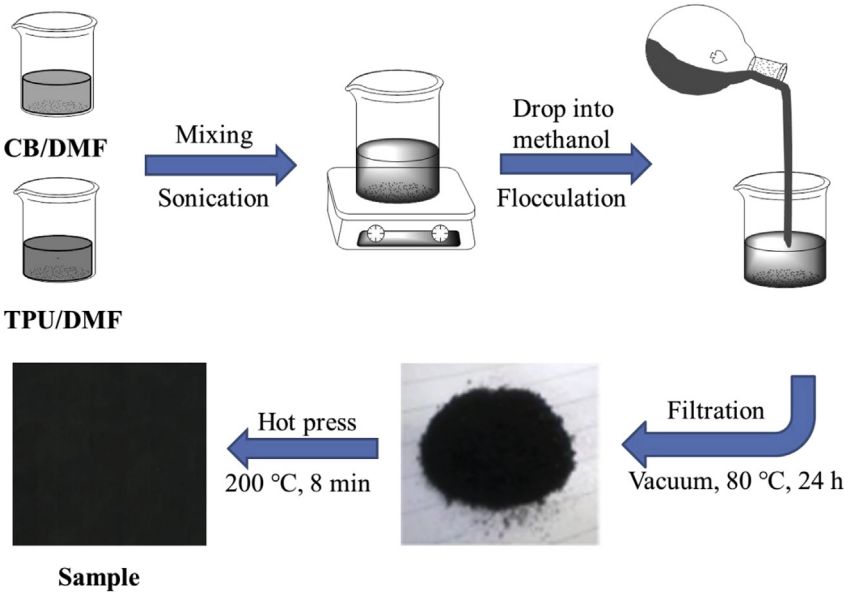

Fig. 1. Schemes of the process for the fabrication of CB/TPU nanocomposites by the co-coagulation technique and hot pressing.

20 mL/min using a TA instruments Q 2000. The samples were heated from 40 to 220 °C at a heating rate of 10 °C min^{-1} (to eliminate the thermal history, all samples were held isothermally for 5 min at 220 °C), then cooled down to −70 °C and reheated to 220 °C at the same rate.

The samples for mechanical tests were 40 mm × 4 mm × 0.4 mm and conducted on an electrical universal testing instrument with a 100 N load cell (UTM2203). All samples were tested with a strain of 0.1 min^{-1} using an initial grip-to-grip separation of 16 mm under ambient conditions, as performed previously [31]. Each sample was tested as least five times to ensure repeatability.

For the morphology characterization of CB in TPU, tensile fracture cross section and eroded surfaces were inspected using field emission scanning electron microscopy (FE-SEM). All samples were sputtered with a thin layer of platinum to ensure clear imaging.

Thermal conductivity tests were measured using a TPS2200 Hot Disk instrument (AB Corporation, Sweden) by standard methods. A heat pulse of 0.03 W was supplied by the sensor (3.2 mm diameter) to the sample for 20 s and the thermal conductivity of the sample was obtained. Each sample was tested as least five times to ensure repeatability.

Thermal stability was carried out using TGA (TA instruments, Q50) at a heating rate of 10 °C min^{-1} from ambient temperature to 700 °C in nitrogen atmosphere. The nitrogen flow rate was 40 mL/min. Each sample was tested as least five times to ensure repeatability.

All solid particle erosion tests were performed in a commercial sand-blasting machine (BH-1350, Shenzhen Datong Sand-blasting Machine Co., Ltd, China). The samples with dimensions of 20 mm × 4 mm × 0.4 mm were cut from the CB/TPU nanocomposite films for erosion tests. The erodent was blocky, angular-shaped abrasive green SiC particles, obtained from ChangAn Co., Ltd with mean diameters of 150 μm. Three different impact angles were used (30°, 60° and 90°) for this test. Different impact velocities were obtained using different air pressures in the nozzle, determined using the double disc method [49]. The solid particle erosion behavior was characterized by the ER defined from the following formula [49]:

$$ER = \frac{W_m}{W_p} \quad (1)$$

where W_m is the weight loss of the tested sample and W_p is the mass of the erodent particles (testing time × erodent feed rate). The weight of the sample before and after solid particle erosion test was recorded using an electronic balance. Each sample was tested as least five times to ensure repeatability.

3. Results and discussion

3.1. Interfacial interaction between CB and TPU

CB contains −OH, C═O and −COOH groups, which easily form hydrogen bonds with the urethane and ester groups of TPU [57]. Meanwhile, the hydrogen bonding between nanoparticles and polymer chains could effectively enhance the mechanical properties of the nanocomposites [58]. In this study, the FT-IR spectra of all samples are shown in Fig. S1. In the CB/TPU nanocomposites, the presence of hydrogen bonding will influence the strength of the C═O bonds of TPU. Hence, the hydrogen bonding index (R) of TPU, defined as the ratio of peak intensity of the C═O at 1700 cm^{-1} to C═O at 1730 cm^{-1}, was used to confirm the presence of hydrogen bonding between CB and TPU [59]. As shown in Fig. 2 (a), R increases with increasing the CB content from 2 to 10 wt%, indicating the existence of hydrogen bonding. However, there is no obvious change in R for TPU-10CB and TPU-12CB, which may be due to the aggregation of the CB particles at a higher loading, hindering the formation of extra hydrogen bonding. It is theorized that this phenomenon may have a dramatic effect on the mechanical performance of the CB/TPU nanocomposites.

Apart from FT-IR, the glass transition temperature (T_g) is also frequently used to evaluate the interaction between filler and polymer matrix [60]. Fig. 2 (b) displays the DSC curves of all samples. From Fig. 2 (b), the T_g decreases from −27.35 °C for neat TPU to −30.37 °C for TPU-12CB. The T_g of the nanocomposites depends on the mobility of TPU soft segment molecules. The entanglement degree of the soft chains of TPU may be reduced in the presence of CB, causing a higher mobility of soft segments. In addition, the destruction of the crystalline structure of hard segments, which act as physical crosslinking points of the TPU molecules, will release the constrained soft segments and improve its mobility. Hence, the reduction of T_g also confirms the interaction between CB and TPU matrix. Similar phenomena have also been reported in other systems [32,61].

3.2. Mechanical properties of CB/TPU nanocomposites

Fig. 3 shows the representative stress-strain curves of all the samples. A CB filled TPU should be regarded as a composite characterized by a “rubbery” continuous phase and a particulate “rigid” dispersed

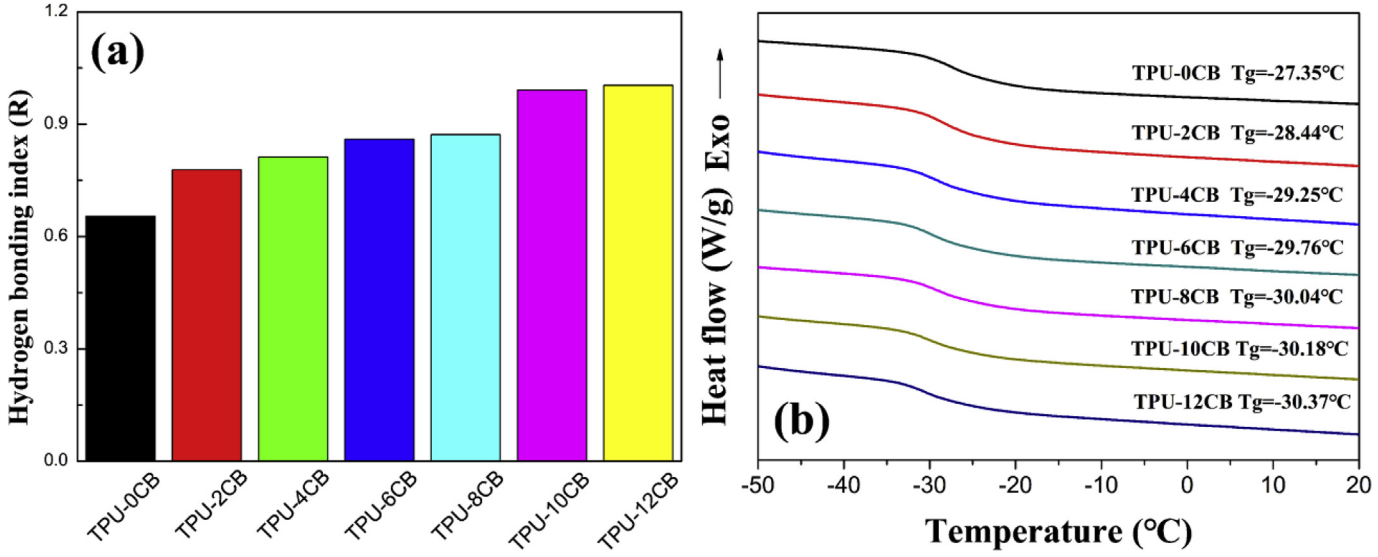

Fig. 2. (a) Hydrogen bonding indexes (*R*), and (b) DSC curves of tested samples.

phase. When the nanocomposite is stretched, the tensile stress tends to transfer from the substrate to the interface between the CB particles and the TPU matrix and can be further transferred to boundary deformation energy [62,63]. When CB is dispersed in the TPU matrix, substantial changes are observed in the tensile properties of the nanocomposites compared to neat TPU. The tensile strength of TPU-2CB is 3.356 MPa, which is lower than that of neat TPU (4.688 MPa). This is due to the fact that a small amount of CB particles could not strengthen the TPU effectively. On one hand, a lower CB loading cannot constitute a complete three-dimensional network throughout the TPU matrix, when the tensile stress is transmitted to the interface between the CB particles and the TPU matrix, the local stress concentration is formed, causing crack propagation and reducing the tensile strength of the nanocomposite. On the other hand, the existence of low CB loading destroys the TPU molecular chain structure, causing the reduction of mechanical properties [64]. In addition, the tensile strength of TPU-4CB, TPU-6CB and TPU-8CB was observed to be 4.794, 5.404 and 5.576 MPa, respectively. The improved properties are mainly due to the homogenously distributed CB nanoparticles in the TPU matrix. However, both TPU-10CB and TPU-12CB did not show obviously enhanced mechanical properties compared with TPU-4CB, and the tensile strength of TPU-10CB and TPU-12CB was 4.890 and 4.844 MPa, respectively. This phenomenon is mainly attributed to the agglomeration of CB particles with an increased loading, leading to increased interfacial defects.

The uniform dispersion of CB particles in TPU is very important to acquire high-quality nanocomposites. To clearly understand the corollaries above, freeze-fractured surfaces of CB/TPU nanocomposites were collected to characterize the dispersion state of CB particles (Fig. 4(a) and (b)). As shown in Fig. 4 (a), the surface of TPU-6CB displays a “river-like” pattern, and the CB nanoparticles are homogenously distributed in the TPU matrix. For TPU-12CB, the agglomeration of CB nanoparticles is observed and is marked by red circles in Fig. 4 (b). Compared with the TPU-6CB, the density of the “river-like” pattern appeared to be increased in the SEM image of the TPU-12CB. It is known that the “river-like” structure arises from the cracks caused by agglomerated CB nanoparticles. Hence, the increased density of “river-like” structure illustrates the existence of CB agglomeration, which leads to the fracture of composites. In addition, the morphologies of tensile broken section of TPU-6CB and TPU-12CB were also analyzed, seen in Fig. 4(c) and (d). The tensile broken section of TPU-6CB is very rough with dimple pores, and the material exhibits tough fracture. On the contrary, in Fig. 4 (d), the tensile broken section of TPU-12CB is smoother than TPU-6CB, arising from the fact that the fracture crack usually occurs at the agglomerated CB particles [65]. It is known that the kinetic energy and strain potential of the crack tip can be transformed into non-continuous boundary deformation energy. The evenly

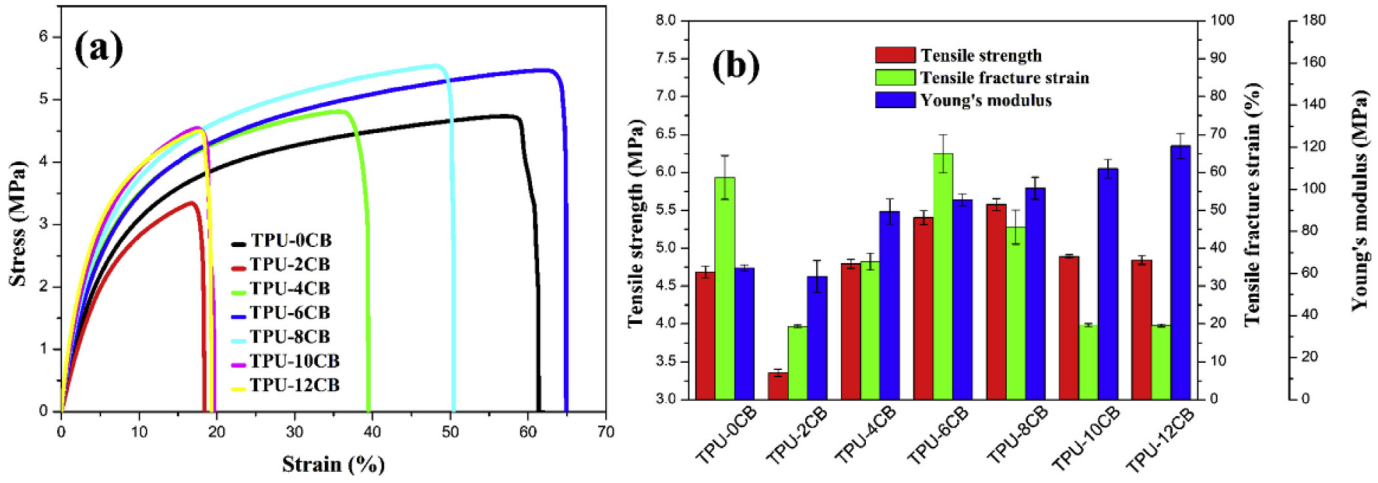

Fig. 3. (a) Representative stress-strain curves, and (b) mechanical properties of TPU nanocomposites as a function of CB loading.

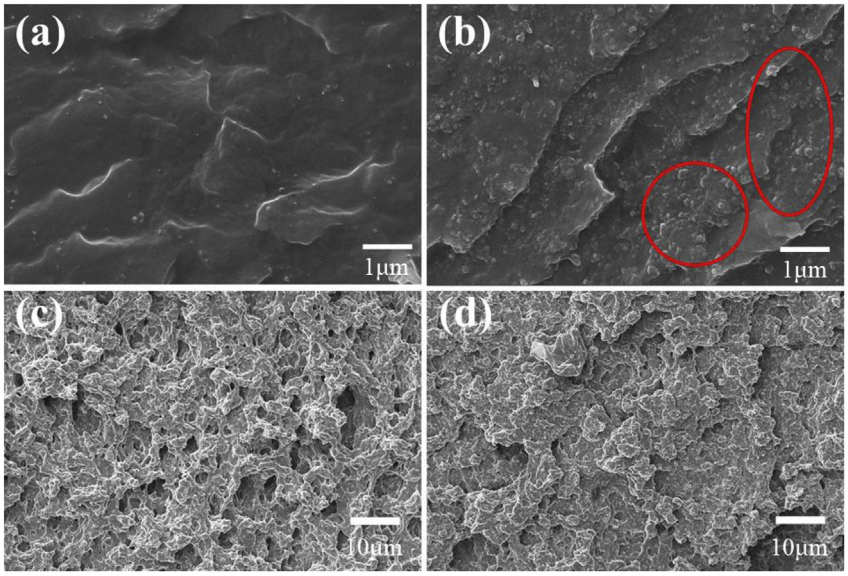

Fig. 4. FE-SEM images of the freeze-fractured surface of (a) TPU-6CB, (b) TPU-12CB, and the tensile broken section of (c) TPU-6CB, and (d) TPU-12CB.

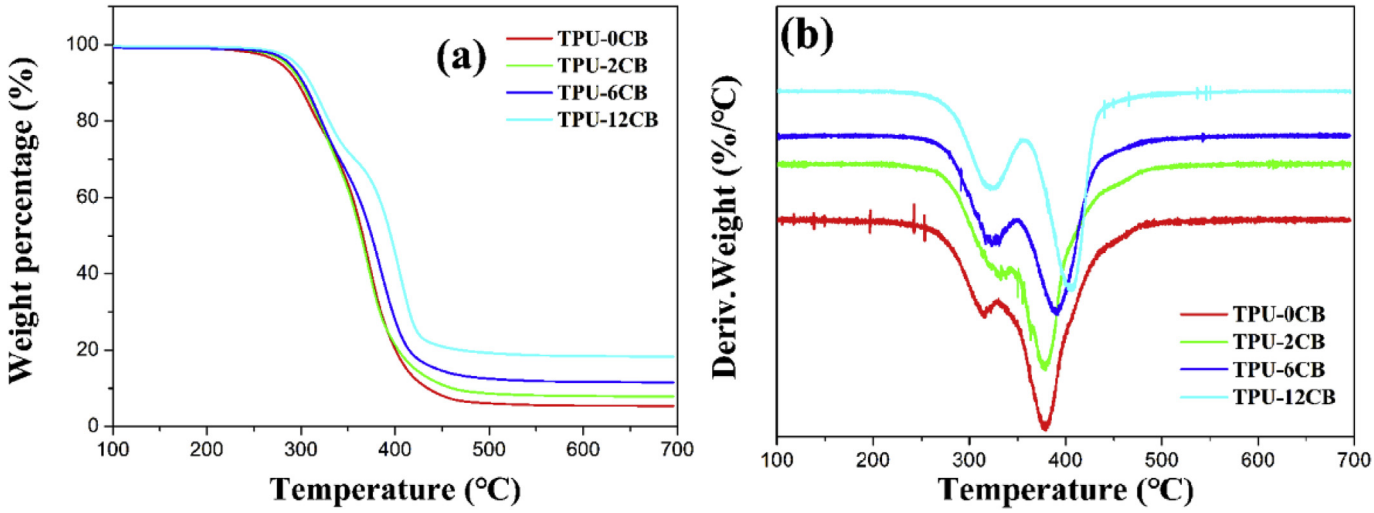

Fig. 5. (a) TGA and (b) DTG curves of the tested samples.

Table 1
Thermal conductivity and thermogravimetric analysis data of CB/TPU nanocomposites.

sample	thermal conductivity (W/mK)	$T_{5\%}$/°C	$T_{10\%}$/°C	T_{max}/°C
TPU-0CB	0.27	278.58	296.32	366.92
TPU-2CB	0.30	284.92	300.48	367.17
TPU-6CB	0.34	287.93	302.73	386.07
TPU-12CB	0.36	295.23	309.88	403.24

dispersed CB particles can play a vital role in promoting the deflection and separation of cracks when the CB/TPU nanocomposites are subjected to stress. Here, the surface layer between the nanoparticles and the polymer matrix can also suppress the growth of cracks. On the other hand, when the CB nanoparticles and the TPU chains are linked together forming three-dimensional networks through the interfacial layer, the CB nanoparticles serve as cross-linking points and can uniformly distribute the stress to reduce the material damage. The appropriate CB content plays a vital role in improving the mechanical performance of the nanocomposites. Fig. 4 provides an evidence for the increased mechanical properties for the TPU-6CB.

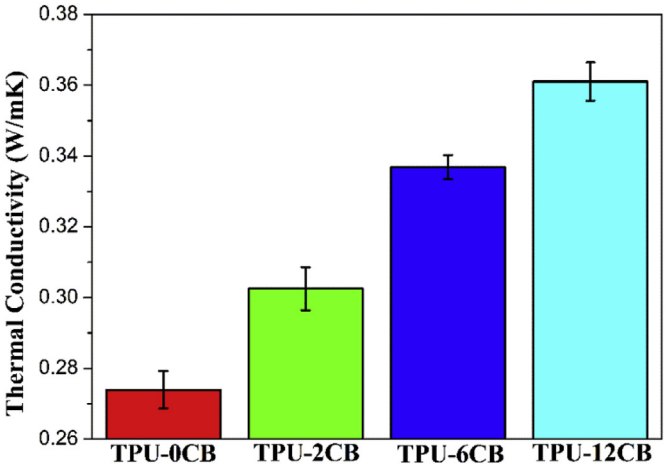

Fig. 6. Thermal conductivity of the tested samples.

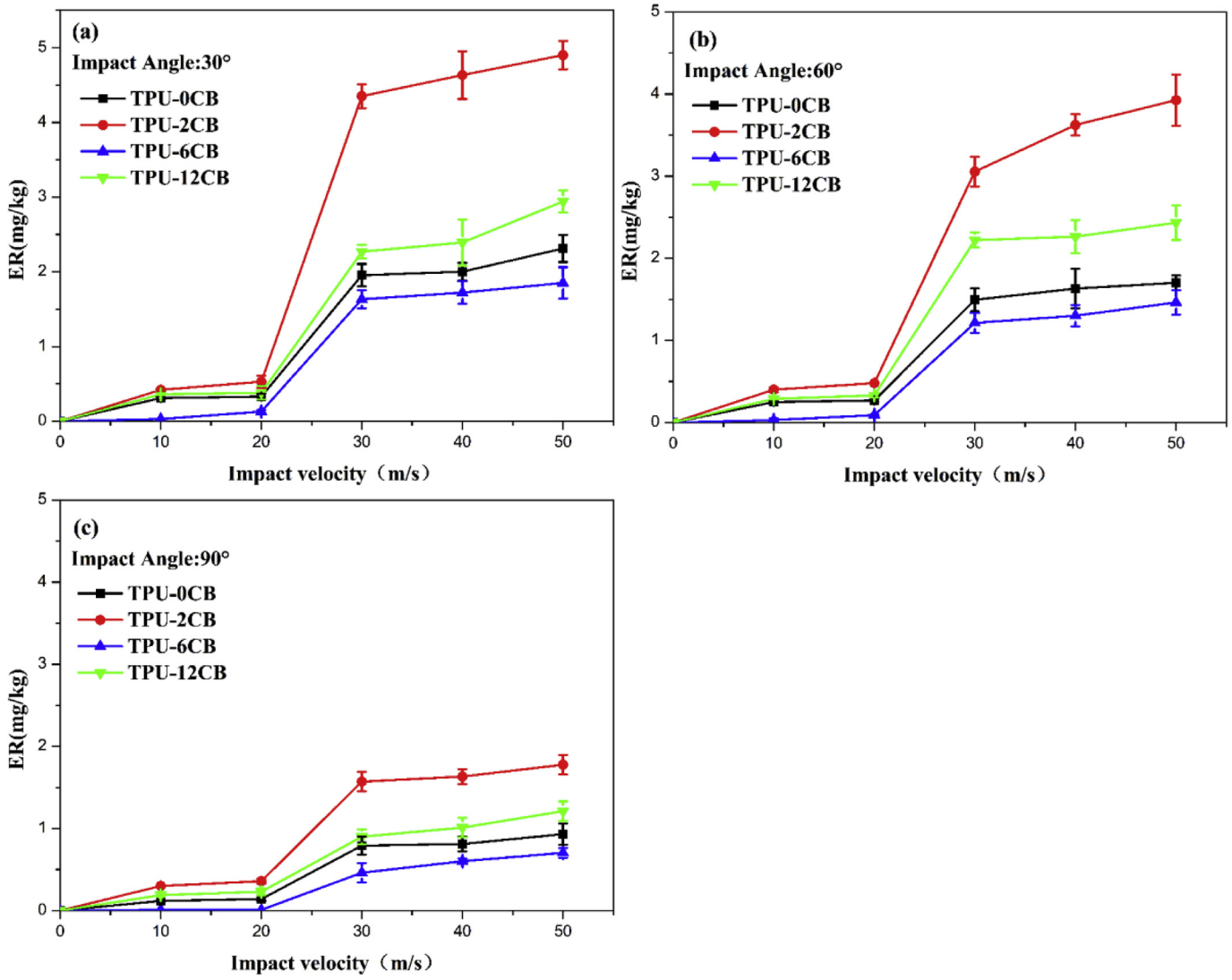

Fig. 7. Erosion rate (ER) of tested samples as a function of impact velocity at (a) 30°, (b) 60° and (c) 90° impact angles with the impact time of 300 s.

As shown in Fig. 3 (b), the Young's modulus is increased with increasing the CB content, due to high rigidity of CB particles [65]. The Young's modulus is increased by 92.6% from 62.6 MPa for neat TPU to 120.6 MPa for the TPU-12CB. Moreover, the variation in the elongation at break shows the same trend as the observed tensile strength. It is known that the CB nanoparticles have high rigidity and are not easily deformed, so the elongation of the nanocomposites under stress mainly depends on the TPU matrix. The reduced elongation at break of nanocomposites with lower CB loadings is due to the fact that a lower CB loading cannot constitute a complete three-dimensional network throughout the TPU matrix and exist only as defects in the matrix. Due to the homogeneous dispersion of CB nanoparticles in TPU, the elongation at break of TPU-6CB was improved. When the content of CB nanoparticles is moderate to form a three-dimensional network structure, the uniform distribution of stress on the CB nanoparticles can reduce the probability of breakages in a single molecular chain, so an increase in the elongation at break is obtained. With further increasing the CB loading, a gradually decreasing trend in the elongation at break was observed. This is attributed to the agglomeration of CB particles becoming more pertinent at higher CB loadings, where the deformation of TPU is limited. In the subsequent experiments, we selected representative samples of mechanical properties for testing. Neat TPU was compared with the samples with the worst tensile strength (TPU-2CB), the best elongation at break (TPU-6CB), and the highest Young's modulus (TPU-12CB).

3.3. Thermal stability of the CB/TPU nanocomposites

The TGA and DTG curves of tested samples are shown in Fig. 5(a) and (b) and Table 1. In Fig. 5 (a), the weight loss at different temperatures of CB/TPU nanocomposites has a similar trend. The initial decomposition temperature (temperature at 5% and 10% mass loss, simplify to $T_{5\%}$ and $T_{10\%}$, respectively) of the CB/TPU nanocomposites increased with the addition of CB as compared with pure TPU. An enhancement of 16.65 and 13.56 °C was observed for the TPU-12CB, respectively. Two peaks were observed from the curves in Fig. 5 (b). The first peak is due to the break of urethane bonds, and the other peak is due to the degradation of the TPU chains [32]. The largest thermal decomposition temperature (T_{max}) increased with increasing the CB content. Compared with neat TPU, the T_{max} of thermal decomposition rate of TPU-12CB was increased by 36.32 °C. Thus, the CB particles are beneficial for improving the thermal stability of the nanocomposites.

3.4. Thermal conductivity of the CB/TPU nanocomposites

The thermal conductivity of all tested samples can be seen in Fig. 6 and Table 1. With increasing the CB loading, the thermal conductivity of CB/TPU nanocomposites exhibits an increasing trend. Compared

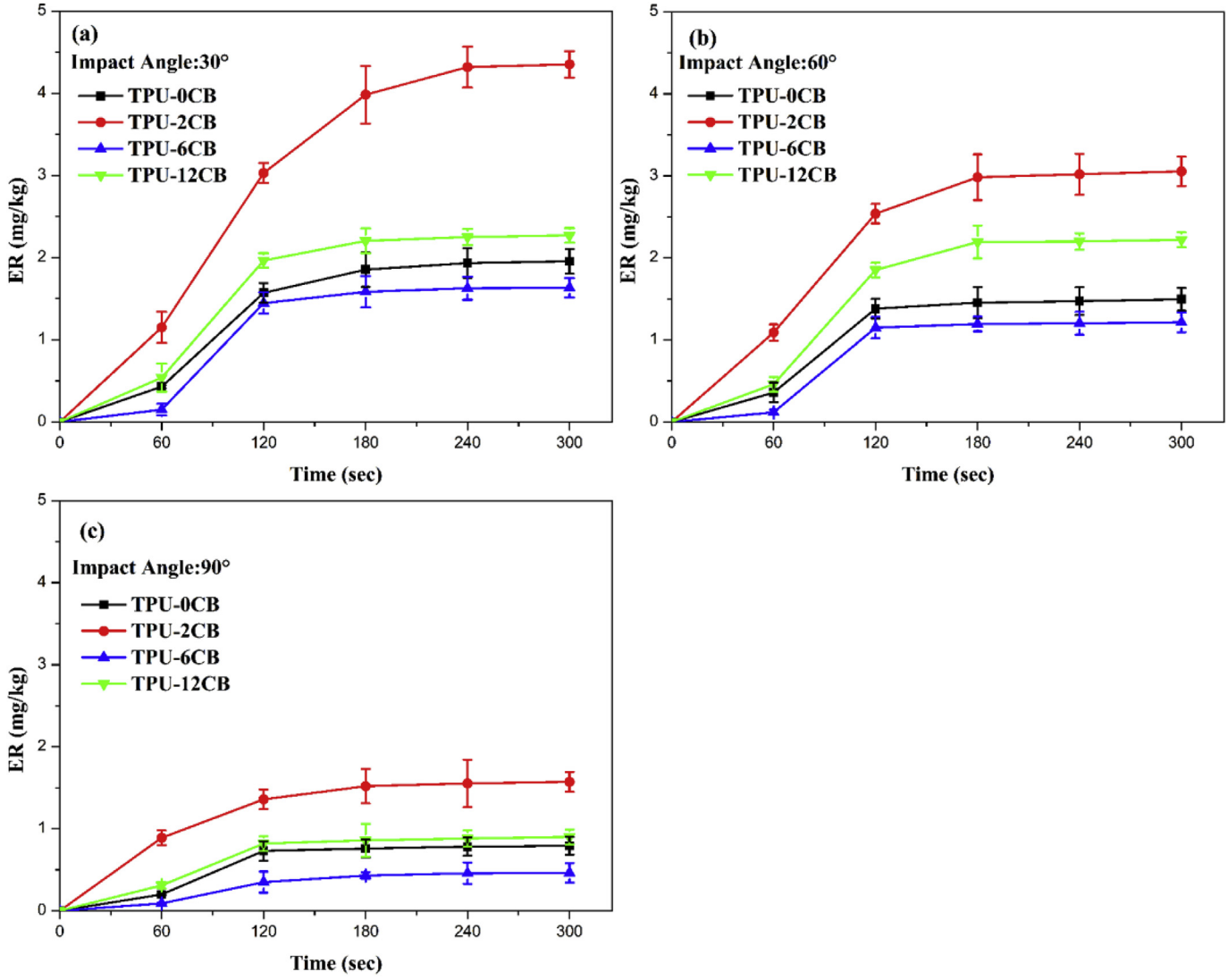

Fig. 8. Erosion rate (ER) of tested samples as a function of erosion time at (a) 30°, (b) 60° and (c) 90° impact angles with the impact velocity at 30 m/s.

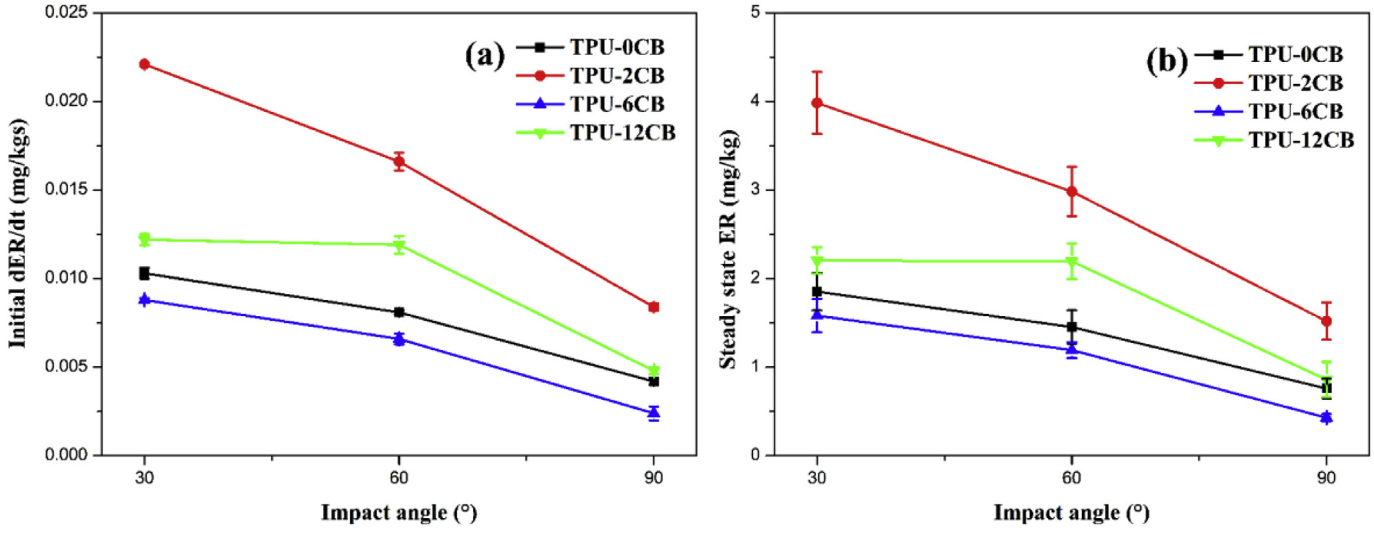

Fig. 9. (a) ER initial slope, and (b) steady state ER of tested samples as a function of impact angle.

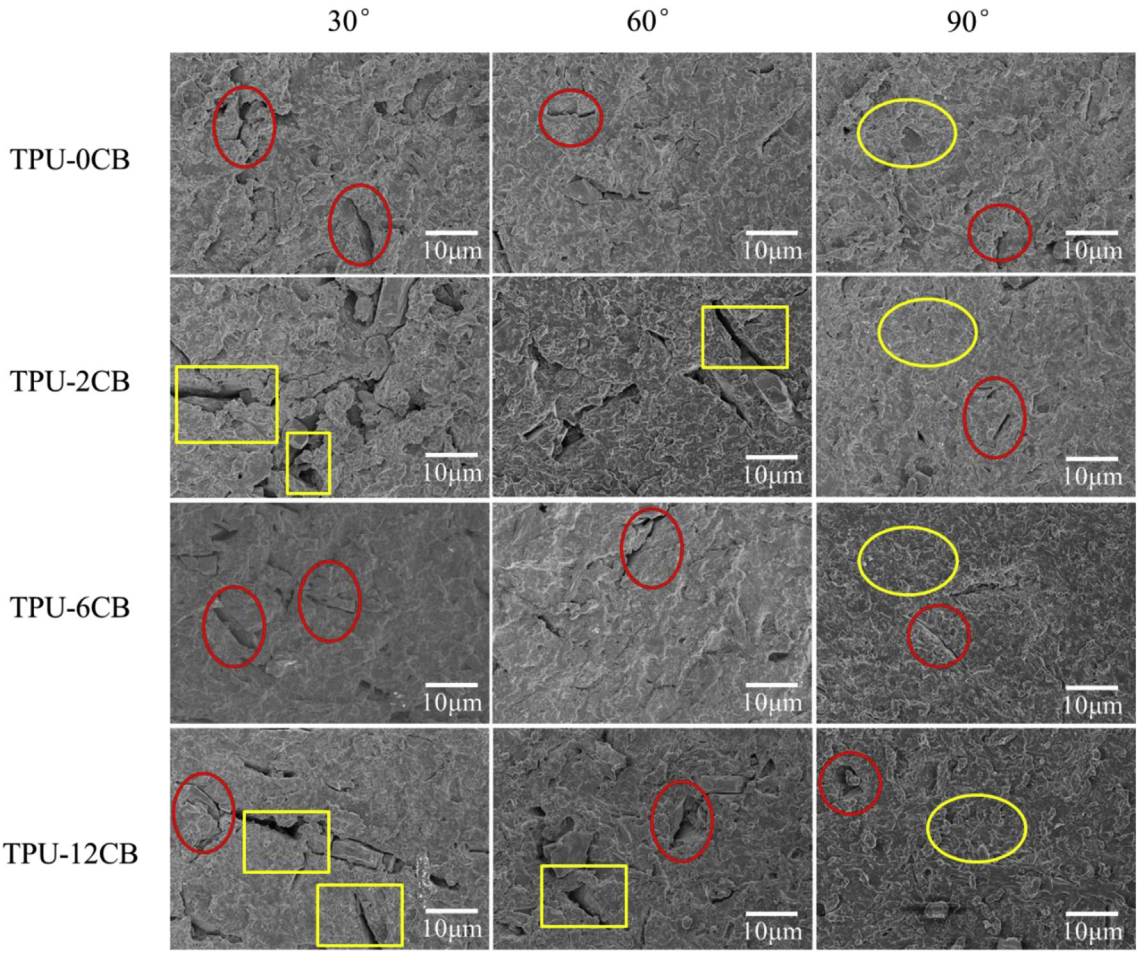

Fig. 10. FE-SEM images of CB/TPU nanocomposites after solid particle erosion of impact velocity at 30 m/s with the impact time of 300 s.

with neat TPU, the thermal conductivity of TPU-12CB is increased by 33.3%. This is due to the formation of thermal conductivity phases with increasing the CB loading. The surface temperature of the nanocomposites will increase with progressing the solid particle erosion process, and high temperatures may damage the surface of the material. The improved thermal conductivity is beneficial for the conduction of heat generated during the solid particle erosion processes, thus an appropriate CB content can improve the wear resistance of the nanocomposites.

3.5. Solid particle erosion behavior of the CB/TPU nanocomposites

Within the impact time of 300 s at three different angles of impingement (30°, 60° and 90°), the ER of all samples as a function of impact velocity was investigated, and the findings are illustrated in Fig. 7. At a low velocity, the solid particles may produce only elastic stress on the surface of CB/TPU nanocomposites and hence the ER is smaller than that at higher velocities. In addition, irrespective of the impingement angles and CB loading, the ER of all samples presents an abrupt increase with the impact velocity between 20 and 30 m/s. The ER of the nanocomposites reached a steady state with further increasing the impact velocity. The maximum ER of all CB/TPU nanocomposites is observed at 30°, indicating a typical ductile erosion behavior (maximum erosion rate of brittle and ductile materials is usually achieved at about 90° and 30° impact angle, respectively) [66].

As for the impact velocity of 30 m/s at 30°, 60° and 90°, the ER values of all samples as a function of erosion time are studied and displayed in Fig. 8. All the CB/TPU nanocomposites reach a steady state after 180 s. Based on Fig. 8, the dER/dt is defined as the slope of the linear part of the curves. As shown in Fig. 9, the initial dER/dt and the steady ER for all the samples show the same trends as the maximum values at 30° and minimum values at 90°. This suggests that the CB/TPU nanocomposites possess the highest ER when the impingement angle is nearly parallel to the surface. Among different CB/TPU nanocomposites, the TPU-6CB showed the lowest ER, and the TPU-2CB exhibited the highest ER.

The failure mode for CB/TPU nanocomposites is complex, involving surface matrix removing, surface micro cracking, fracture, chipping off, and material removal. The ridges were usually formed at the initial stage of particles impacting. Once a steady state condition was achieved under the high impact velocities, small cracks and a high degree of plastic deformation occurred. The ridges would be deformed during the successive impact process, which caused some cracks in a direction perpendicular to the erosion direction, and then started to grow at the ridge base [67]. Fracture and chipping of the surface are ascribed to the succession of impacts, and the strain gradually increases until the removal of the material occurred. In this way, the cyclic impact causes the crack growth and expansion, causing the material loss [68].

The eroded surfaces of CB/TPU nanocomposites were observed under SEM to investigate the erosion mechanism. All the aforementioned features can be found for all the CB/TPU nanocomposites under an impact velocity of 30 m/s within 300 s at three different angles of impingement (30°, 60° and 90°), Fig. 10. The force of impact is known to be divided into two parts (parallel to the surface (F_p), and vertical to the surface (F_v)) when the impact angle is tilted [69]. The F_p influences the cutting and plowing, and F_v controls the impact. Generally, F_p plays a more important role than F_v in the erosion for ductile materials [70]. The impact force at 30° has a higher F_p on the surface than that at 60°.

As shown in Fig. 10, some plastic deformations are reflected and marked by yellow circles, some micro-plowing and micro-cracks are observed and marked by red circles, the deep cracks are marked by yellow rectangles. The micro-plowing, micro-cracks and plastic deformation caused by the impact particles are similar at the impingement angles of 30° and 60°, but it is more obvious at 30°. However, there is almost no micro-plowing, micro-cracks due to the zero F_p at 90° impingement angle. Hence, the maximum erosion rate is achieved at about 30° impact angle for ductile materials, which is consistent with the ER value. Compared with other CB/TPU nanocomposites, TPU-2CB suffered severe erosion at three different impact angles. Similar to other tribological procedures, the enhancement of mechanical properties is always coincident with superior erosion resistance. The poor erosion resistance of TPU-2CB is due to its poor mechanical properties. The TPU-2CB nanocomposites have the lowest tensile strength and relatively low modulus, it is easier to reach the critical value of material damage under the same solid particle erosion test conditions compared with other nanocomposites. It is consistent with the lowest erosion resistance as shown in Fig. 9.

4. Conclusion

CB/TPU nanocomposites were manufactured by a co-coagulation technique and hot pressing. Homogeneous dispersion of CB in TPU matrix was observed due to the existence of hydrogen bonding interactions between them, which was also identified by the decrease of T_g from −27.35 °C for neat TPU to −30.37 °C for TPU-12CB. These are beneficial for the significantly enhanced mechanical properties of the TPU-6CB nanocomposites, as compared to neat TPU. The thermal conductivity and thermal stability of the CB/TPU nanocomposites were observed to be improved with increasing the CB content. As for the solid particle erosion behavior of CB/TPU nanocomposites, the influences of CB content, impact angle, and velocity on the wear resistance behavior were investigated systematically. The results showed that the solid particles would only bring elastic stress to the surface of CB/TPU nanocomposites at a sufficiently low velocity, and all the samples exhibited a rapid increasing of ER with the impact velocity between 20 and 30 m/s. The maximum and minimum ER was observed at 30° and 90° impact angle for all the CB/TPU nanocomposites, respectively, showing a typical ductile erosion behavior. In addition, the ER (TPU-2CB > TPU-12CB > TPU > TPU-6CB) showed an opposite trend as the tensile strength. In brief, due to the uniform dispersion of CB in TPU at a suitable CB content, the CB/TPU nanocomposites achieved a better wear resistance than neat TPU. This study indicates that the CB/TPU nanocomposites are appropriate to serve as protective coatings, which can strongly limit the occurrences of erosion processes in environments where high speed particles may attack the surfaces.

Acknowledgements

This work was supported by the China Scholarship Council (CSC) program. C. L. and H. L. acknowledge the financially support from NSFC (11572290, 51803191).

Appendix A. Supplementary data

Supplementary data to this article can be found online at https://doi.org/10.1016/j.polymer.2018.11.003.

References

[1] A. Patnaik, A. Satapathy, N. Chand, N.M. Barkoula, S. Biswas, Solid particle erosion wear characteristics of fiber and particulate filled polymer composites: a review, Wear 268 (2010) 249–263.
[2] Y. Huang, Z. Zhang, J. Xu, L. Xu, G. Zhong, B. He, Z. Li, Simultaneously improving wear resistance and mechanical performance of ultrahigh molecular weight polyethylene via cross-linking and structural manipulation, Polymer 90 (2016) 222–231.
[3] J. Barrioz, D. Mazuyer, P. Kapsa, A. Chateauminois, G. Robert, Abrasive wear micro mechanisms of oriented polymers, Polymer 45 (2004) 2729–2736.
[4] L. Jiang, C. He, J. Fu, D. Chen, Wear behavior of straw fiber-reinforced polyvinyl chloride composites under simulated acid rain conditions, Polym. Test. 62 (2017) 373–381.
[5] O. Reynolds, On the action of a blast of sand in cutting hard materials, Philos. Mag. A 46 (1873) 337–343.
[6] J.W.S. Rayleigh, The sand blast, Nature 93 (1912) 188.
[7] Y.I. Oka, H. Ohnogi, T. Hosokawa, M. Matsumura, The impact angle dependence of erosion damage caused by solid particle impact, Wear 203–204 (1997) 573–579.
[8] R. Rattan, J. Bijwe, Influence of impingement angle on solid particle erosion of carbon fabric reinforced polyetherimide composite, Wear 262 (2007) 568–574.
[9] S. Arjula, A.P. Harsha, Study of erosion efficiency of polymers and polymer composites, Polym. Test. 25 (2006) 188–196.
[10] M. AminulIslam, Z.N. Farhat, Effect of impact angle and velocity on erosion of API X42 pipeline steel under high abrasive feed rate, Wear 311 (2014) 180–190.
[11] D. Mitramajumdar, H. Aglan, Behaviour of advanced polymer composites in erosive/corrosive environments, Polymer 33 (1992) 1855–1859.
[12] P.H. Shipway, I.M. Hutchings, A method for optimizing the particle flux in erosion testing with a gas-blast apparatus, Wear 174 (1994) 169–175.
[13] L.W. Mckeen, The Effect of Temperature and Other Factors on Plastics and Elastomers, William Andrew Inc., NY, 2008.
[14] A. Kishore, G.B. Sridhar, On evaluating erosion by sand particles in polythene system without and with ceramic particles, Polym. Test. 21 (2002) 473–477.
[15] G.K. Drensky, Experimental Investigation of Composite Material, Erosion Characteristics under Conditions Encountered in Turbofan Engines, Doctor of Philosophy M.S University of Cincinnati, Cincinnati, Ohio, 2002.
[16] A. Patnaik, A. Satapathy, S.S. Mahapatra, R.R. Dash, A modelling approach for prediction of erosion behavior of glass fiber-polyester composites, J. Polym. Res. 15 (2) (2008) 147–160.
[17] A. Patnaik, A. Satapathy, S.S. Mahapatra, R.R. Dash, Tribo-performance of polyester hybrid composites: damage assessment and parameter optimization using Taguchi design, Mater. Des. 30 (2009) 57–67.
[18] P.J. Slikkerveer, M.H.A. Dongen, F.J. Touwslager, Erosion of elastomeric protective coatings, Wear 236 (1999) 189–198.
[19] Z. Bartczak, M. Grala, E. Richaud, K. Gadzinowska, Erosion of the molecular network in the amorphous layers of polyethylene upon high-strain deformation, Polymer 99 (2016) 552–565.
[20] R. Kaundal, Role of process variables on solid particle erosion of polymer composites: a critical review, Siliconindia 9 (2017) 223–238.
[21] C. Wang, M. Zhao, J. Li, J. Yu, S. Sun, S. Ge, X. Guo, F. Xie, B. Jiang, E. Wujcik, Y. Huang, N. Wang, Z. Guo, Silver nanoparticles/graphene oxide decorated carbon fiber synergistic reinforcement in epoxy-based composites, Polymer 131 (2017) 263–271 https://doi.org/10.1016/j.polymer.2017.10.049.
[22] S. Biswas, A. Satapathy, A comparative study on erosion characteristics of red mud filled bamboo–epoxy and glass–epoxy composites, Mater. Des. 31 (2010) 1752–1767.
[23] N. Zhang, F. Yang, L. Li, C. Shen, J. Castro, L. James Lee, Thickness effect on particle erosion resistance of thermoplastic polyurethane coating on steel substrate, Wear 303 (2013) 49–55.
[24] J.W.M. Mens, A.W.J. De Gee, Erosion in weawater sand slurries, Tribol. Int. 19 (1986) 59–64.
[25] S. Soderberg, S. Hogmark, U. Engman, H. Swahn, Erosion classification of materials using a centrifugal erosion tester, Tribol. Int. 14 (1981) 333–343.
[26] M. Su, X. Zeng, X. Lai, H. Li, Effect of mixing sequences of γ-piperazine propylmethyl dimethoxysilane on the tracking and erosion resistance of silicone rubber, Polym. Test. 65 (2018) 491–496.
[27] X. Cui, G. Zhu, Y. Pan, Q. Shao, C. Zhao, M. Dong, Y. Zhang, Z. Guo, Polydimethylsiloxane-titania nanocomposite coating: fabrication and corrosion resistance, Polymer 138 (2018) 203–210 https://doi.org/10.1016/j.polymer.2018.01.063.
[28] A.S. Virk, W. Hall, J. Summerscales, Failure strain as the key design criterion for fracture of natural fibre composites, Compos. Sci. Technol. 70 (2010) 995–999.
[29] (a) G. Arena, K. Friedrich, D. Acierno, E. Padenko, P. Russo, G. Filippone, J. Wagner, Solid particle erosion and viscoelastic properties of thermoplastic polyurethanes, Express Polym. Lett. 9 (2015) 166–176;
(b) C. Wang, Y. Wu, Y. Li, Q. Shao, X. Yan, C. Han, Z. Wang, Z. Liu, Z. Guo, Flame retardant rigid polyurethane foam with a phosphorus-nitrogen single intumescent flame retardant, Polym. Adv. Technol. 29 (2018) 668–676.
[30] Y. Yang, P. Zeng, L. Lei, Numerical simulation study of the T-peel behavior of coated fabric films used in inflatable structures, J. Appl. Polym. Sci. 132 (3) (2015) 41299.
[31] (a) H. Liu, Y. Li, K. Dai, G. Zheng, C. Liu, C. Shen, X. Yan, J. Guo, Z. Guo, Electrically conductive thermoplastic elastomer nanocomposites at ultralow graphene loading levels for strain sensor applications, J. Mater. Chem. C. 4 (2016) 157;
(b) Y. Lu, M.C. Biswas, Z. Guo, J. Jeon, E.K. Wujcik, Recent developments in bio-monitoring via advanced polymer nanocomposite-based wearable strain sensors, Biosens. Bioelectron. 123 (2019) 167–177.
[32] H. Liu, M. Dong, W. Huang, J. Gao, K. Dai, J. Guo, G. Zheng, C. Liu, C. Shen, Z. Guo, Lightweight conductive graphene/thermoplastic polyurethane foams with ultrahigh compressibility for piezoresistive sensing, J. Mater. Chem. C. 5 (2017) 73.
[33] H. Wei, D. Ding, S. Wei, Z. Guo, Anticorrosive conductive polyurethane multiwalled carbon nanotube nanocomposites, J. Mater. Chem. A. 1 (2013) 10805.
[34] (a) J. Guo, H. Song, H. Liu, C. Luo, Y. Ren, T. Ding, M.A. Khan, D.P. Young, X. Liu, X. Zhang, J. Kong, Z. Guo, Polypyrrole-interface-functionalized nano-magnetite epoxy nanocomposites as electromagnetic wave absorber with enhanced flame

retardancy, J. Mater. Chem. C. 5 (2017) 5334;
(b) L. Lv, J. Liu, H. Liu, C. Liu, Y. Lu, K. Sun, R. Fan, N. Wang, N. Lu, Z. Guo, E. Wujcik, An overview of electrically conductive polymer nanocomposites toward electromagnetic interference shielding, Eng. Sci. 2 (2018) 26–42 www.doi.org/10.30919/es8d615;
(c) H. Wu, X. Huang, L. Qian, Preparation, mechanism and property of meta-composites with carbon materials as fillers, Eng. Sci. 2 (2018) 17 www.doi.org/10.30919/es8d656;
(d) L. Wang, H. Qiu, C. Liang, P. Song, Y. Han, Y. Han, J. Gu, J. Kong, D. Pan, Z. Guo, Electromagnetic interference shielding MWCNT-Fe3O4@Ag/epoxy nanocomposites with satisfactory thermal conductivity and high thermal stability, Carbon 141 (2019) 506–514 https://doi.org/10.1016/j.carbon.2018.10.003.

[35] Z. Zheng, O. Olayinka, B. Li, 2S-Soy protein-based biopolymer as a non-covalent surfactant and its effects on electrical conduction and dielectric relaxation of polymer nanocomposites, Eng. Sci. (2018), https://doi.org/10.30919/es8d766 in press.

[36] P. Hou, R. Li, Q. Li, N. Lu, K. Wang, M. Liu, X. Cheng, S. Shah, Novel super-hydrophobic cement-based materials achieved by construction of hierarchical surface structure with FAS/SiO_2 hybrid nanocomposites, ES Mater. Manufac. (2018), https://doi.org/10.30919/esmm5f125 in press.

[37] (a) B. Zhao, C. Zhao, M. Hamidinejad, C. Wang, R. Li, S. Wang, K. Yasamin, C.B. Park, Incorporating a microcellular structure into PVDF/graphene–nanoplatelet composites to tune their electrical conductivity and electromagnetic interference shielding properties, J. Mater. Chem. C. 6 (2018) 10292;
(b) B. Zhao, M. Hamidinejad, C. Zhao, R. Li, S. Wang, Y. Kazemi, C.B. Park, A versatile foaming platform to fabricate polymer/carbon composites with high dielectric permittivity and ultra-low dielectric loss, J. Mater. Chem. (2018), https://doi.org/10.1039/c8ta05556d in press;
(c) H. Gu, H. Zhang, C. Ma, X. Xu, Y. Wang, Z. Wang, R. Wei, H. Liu, C. Liu, Q. Shao, X. Mai, Z. Guo, Trace electrosprayed nanopolystyrene facilitated dispersion of multiwalled carbon nanotubes: simultaneously strengthening and toughening epoxy, Carbon 142 (2019) 131–140;
(d) Z. Wang, R. Wei, J. Gu, H. Liu, C. Liu, C. Luo, J. Kong, Q. Shao, N. Wang, Z. Guo, X. Liu, Ultralight, highly compressible and fire-retardant graphene aerogel with self-adjustable electromagnetic wave absorption, Carbon 139 (2018) 1126–1135.

[38] J. Wang, Z. Shi, X. Wang, X. Mai, R. Fan, H. Liu, X. Wang, Z. Guo, Enhancing dielectric performance of poly(vinylidene fluoride) nanocomposites via controlled distribution of carbon nanotubes and barium titanate nanoparticles, Eng. Sci. (2018), https://doi.org/10.30919/es8d759 in press.

[39] (a) B. Zhao, S. Wang, C. Zhao, R. Li, M. Hamidinejad, Y. Kazemi, C.B. Park, Synergism between carbon materials and Ni chains in flexible poly(vinylidene fluoride) composite films with high heat dissipation to improve electromagnetic shielding properties, Carbon 127 (2018) 469–478;
(b) B. Zhao, C.B. Park, Tunable electromagnetic shielding properties of conductive poly(vinylidene fluoride)/Ni chain composite films with negative permittivity, J. Mater. Chem. C. 5 (2017) 6954;
(c) B. Zhao, C. Zhao, R. Li, S.M. Hamidinejad, C.B. Park, Flexible, ultrathin, and high-efficiency electromagnetic shielding properties of poly(vinylidene fluoride)/carbon composite films, ACS Appl. Mater. Interfaces 9 (2017) 20873–20884.

[40] Dynamic oscillatory rheological properties of polystyrene/poly(methyl methacrylate) blends and their composites in the presence of carbon black, Eng. Sci. 1 (2018) 86–94 www.doi.org/10.30919/es.180402.

[41] (a) J. Zhang, Y. Liang, X. Wang, H. Zhou, S. Li, J. Zhang, Y. Feng, N. Lu, Q. Wang, Z. Guo, Strengthened epoxy resin with hyperbranched polyamine-ester anchored graphene oxide via novel phase transfer approach, Adv. Compos. Hybrid Mater. 1 (2018) 300–309;
(b) H. Du, C. Zhao, J. Lin, Z. Hu, Q. Shao, J. Guo, B. Wang, D. Pan, E.K. Wujcik, Z. Guo, Carbon nanomaterials in direct liquid fuel cells, Chem. Rec. 18 (2018) 1365–1372 https://doi.org/10.1002/tcr.201800008.

[42] H. Unal, A. Mimaroglu, Friction and wear performance of polyamide 6 and graphite and wax polyamide 6 composites under dry sliding conditions, Wear 289 (2012) 132–137.

[43] K. Sun, P. Xie, Z. Wang, T. Su, Q. Shao, J. Ryu, X. Zhang, J. Guo, A. Shankar, J. Li, R. Fan, D. Cao, Z. Guo, Flexible polydimethylsiloxane/multi-walled carbon nanotubes membranous metacomposites with negative permittivity, Polymer 125 (2017) 50–57.

[44] L. Wang, L. Zhang, M. Tian, Mechanical and tribological properties of acrylonitrile-butadiene rubber filled with graphite and carbon black, Mater. Des. 39 (2012) 450–457.

[45] J. Karget-Kocsis, A. Mousa, Z. Major, N. Bekesi, Dry friction and sliding wear of EPDM rubbers against steel as a function of carbon black content, Wear 264 (2008) 359–367.

[46] D. Felhos, J. Karget-Kocsis, Tribological testing of peroxide-cured EPDM rubbers with different carbon black contents under dry sliding conditions against steel, Tribol. Int. 41 (2008) 404–415.

[47] Y. Zhou, F. Pervin, S. Jeelani, P.K. Mallick, Improvement in mechanical properties of carbon fabric-epoxy composite using carbon nanofibers, J. Mater. Process. Technol. 198 (2008) 445–453.

[48] S. Chand, Review carbon fibers for composites, J. Mater. Sci. 35 (2000) 1303.

[49] A. Papadopoulos, G. Gkikas, A.S. Paipetis, N.M. Barkoula, Effect of CNTs addition on the erosive wear response of epoxy resin and carbon fibre composites, Compos. Part A-Appls. 84 (2016) 299–307.

[50] Z. Hu, Z. Wang, B. Fan, X. Qi, J. Mai, D. Gu, Y. Yang, L. Song, Effects of surface-modified graphite on tribological properties and thermal conductivity of fabric self-lubricating liner, Asian J. Chem. (26) (2014) 5712-5716.54.

[51] Y. Chen, D. Li, W. Yang, C. Xiao, M. Wei, Effects of different amine-functionalized graphene on the mechanical, thermal, and tribological properties of polyimide nanocomposites synthesized by in situ polymerization, Polymer 140 (2018) 56–72.

[52] H. Liu, J. Gao, W. Huang, K. Dai, G. Zheng, C. Liu, C. Shen, X. Yan, J. Guo, Z. Guo, Electrically conductive strain sensing polyurethane nanocomposites with synergistic carbon nanotubes and graphene bifillers, Nanoscale 8 (2016) 12977.

[53] W. Cai, X. Feng, W. Hu, Y. Pan, Y. Hu, X. Gong, Functionalized graphene from electrochemical exfoliation for thermoplastic polyurethane: thermal stability, mechanical properties, and flame retardancy, Ind. Eng. Chem. Res. 55 (2016) 10681–10689.

[54] B. Xu, H. Yang, K. Dai, X. Liu, L. Zhang, M. Wang, M. Niu, R. Duan, X. Wang, J. Chen, Thermo-compression-aligned functional graphene showing anisotropic response to in-plane stretching and out-of-plane bending, J. Mater. Sci. 53 (2018) 6574–6585.

[55] Y. Zheng, Y. Li, K. Dai, M. Liu, K. Zhou, G. Zheng, C. Liu, C. Shen, Conductive thermoplastic polyurethane composites with tunable piezoresistivity by modulating the filler dimensionality for flexible strain sensors, Compos. Part A-Appls. 101 (2017) 41–49.

[56] (a) H. Liu, Q. Li, S. Zhang, R. Yin, X. Liu, Y. He, K. Dai, C. Shan, J. Guo, C. Liu, C. Shen, X. Wang, N. Wang, Z. Wang, R. Wei, Z. Guo, Electrically conductive polymer composites for smart flexible strain sensor: a critical review, J. Mater. Chem. C (2018), https://doi.org/10.1039/C8TC04079F in press;
(b) H. Wei, H. Wang, Y. Xia, D. Cui, Y. Shi, M. Dong, C. Liu, T. Ding, J. Zhang, Y. Ma, N. Wang, Z. Wang, Y. Sun, R. Wei, Z. Guo, An overview of lead-free piezoelectric materials and devices, J. Mater. Chem. C (2018), https://doi.org/10.1039/C8TC04515A in press.

[57] Q. Zhang, J. Wang, J. Yu, Z. Guo, Improved electrical conductivity of TPU/carbon black composites by addition of COPA and selective localization of carbon black at the interface of sea-island structured polymer blends, Soft Matter 13 (2017) 3431.

[58] R.W. Seymour, G.M. Estes, S.L. Cooper, Infrared studies of segmented polyurethane elastomers. I. hydrogen bonding, Macromolecules 3 (1970) 579–583.

[59] H. Xia, M. Song, Preparation and characterization of polyurethane-carbon nanotube composites, Soft Matter 1 (2005) 386–394.

[60] Y. Lee, S. Jo, W. Lee, H. Lee, Y.S. Han, D.Y. Ryu, Multiple phase transitions in block copolymer blends and pressure effects on these transitions, Polymer 112 (2017) 427–434.

[61] D.A. Nguyen, Y.R. Lee, A.V. Raghu, H.M. Jeong, C.M. Shin, B.K. Kim, Morphological and physical properties of a thermoplastic polyurethane reinforced with functionalized graphene sheet, Polym. Int. 4 (2009) 412–417.

[62] S. Fu, X. Feng, B. Lauke, Y. Mai, Effects of particle size, particle/matrix interface adhesion and particle loading on mechanical properties of particulate–polymer composites, Compos. B Eng. 39 (2008) 933–961.

[63] S.S. Sternstein, A. Zhu, Reinforcement mechanism of nanofilled polymer melts as elucidated by nonlinear viscoelastic behavior, Macromolecules 35 (2002) 7262–7273.

[64] X. Cao, X. Wei, G. Li, C. Hu, D. Kun, J. Guo, G. Zheng, C. Liu, C. Shen, Z. Guo, Strain sensing behaviors of epoxy nanocomposites with carbon nanotubes under cyclic deformation, Polymer 112 (2017) 1–9.

[65] J. Gong, R. Niu, N. Tian, X. Chen, X. Wen, J. Liu, Z. Sun, E. Mijowska, T. Tang, Combination of fumed silica with carbon black for simultaneously improving the thermal stability, flame retardancy and mechanical properties of polyethylene, Polymer 55 (2014) 2998–3007.

[66] N.M. Barkoula, J. Karget-Kocsis, Review processes and influencing parameters of the solid particle erosion of polymers and their composites, J. Mater. Sci. 37 (2002) 3807–3820.

[67] K.H. Zum Gahr, Wear by hard particles, Tribol. Int. 31 (1998) 587–596.

[68] J. Li, I.M. Hutchings, Resistance of cast polyurethane elastomers to solid particle erosion, Wear 135 (1990) 293–303.

[69] I.M. Hutchings, Mechanisms of wear in powder technology: a review, Powder Technol. 76 (1993) 3–13.

[70] R.G. Wellman, J.R. Nicholls, A review of the erosion of thermal barrier coatings, J. Phys. D Appl. Phys. 40 (2007) 293–305.